Supplement of Atmos. Chem. Phys., 18, 10593–10613, 2018
https://doi.org/10.5194/acp-18-10593-2018-supplement


Atmospheric Chemistry and Physics
Open Access
EGU

*Supplement of*

# Aerosol–cloud interactions in mixed-phase convective clouds – Part 2: Meteorological ensemble

**Annette K. Miltenberger et al.**

*Correspondence to:* Annette K. Miltenberger (a.miltenberger@leeds.ac.uk)

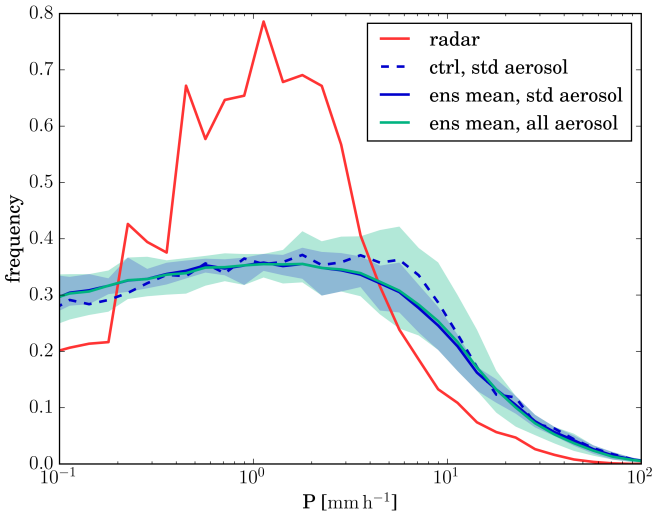


**Figure S1.** Distribution of surface precipitation rate. The distribution considers cloudy grid-points only. The red solid line shows the distribution from radar observation, the dark blue dashed line the distribution from the control run with the standard aerosol profile, the dark blue solid line the mean distribution from all ensemble members with the standard aerosol profile and the cyan line the mean distribution from all ensemble members with all aerosol profiles. The shaded regions display the spread between the ensemble members. Simulated precipitation rates have been coarse-grained to the spatial resolution of the radar observations (1 km horizontal and 500 m vertical).

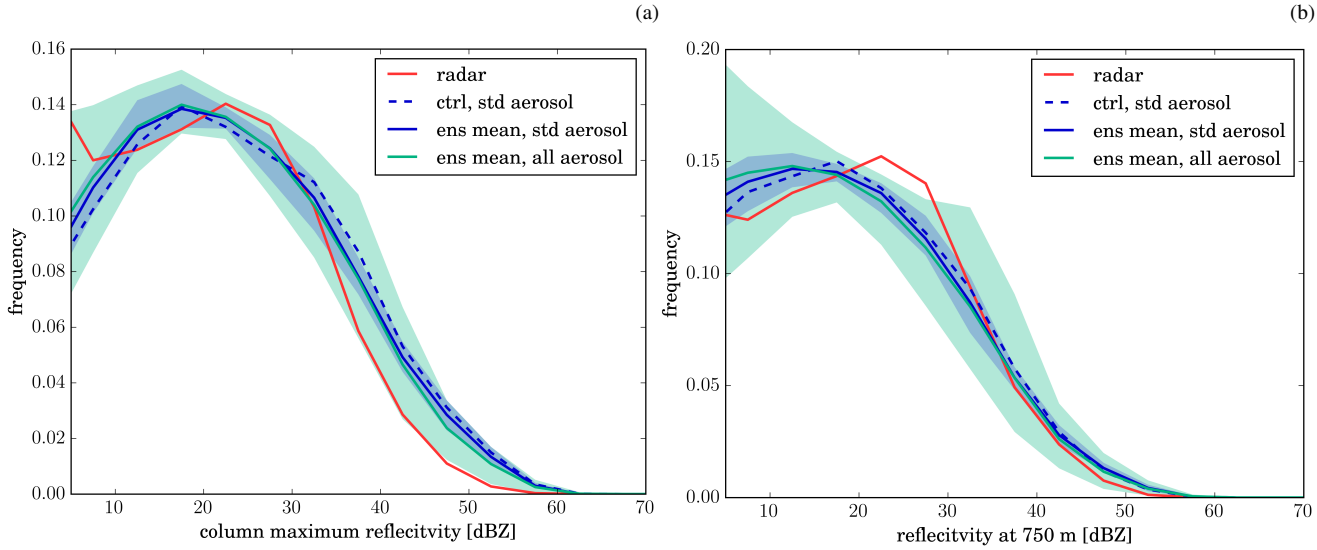


**Figure S2.** Comparison of the distribution of column maximum radar reflectivity (a) and the radar reflectivity at 750 m agl (b) in the model simulations and observational data. The distributions consider cloudy grid-points only. The red solid line shows the distribution from radar observation, the dark blue dashed line the distribution from the control run with the standard aerosol profile, the dark blue solid line the mean distribution from all ensemble members with the standard aerosol profile, and the cyan line the mean distribution from all ensemble members with all aerosol profiles. The shaded regions display the spread between the ensemble members. Simulated radar reflectivity has been coarse-grained to the spatial resolution of the radar observations (1 km horizontal and 500 m vertical).

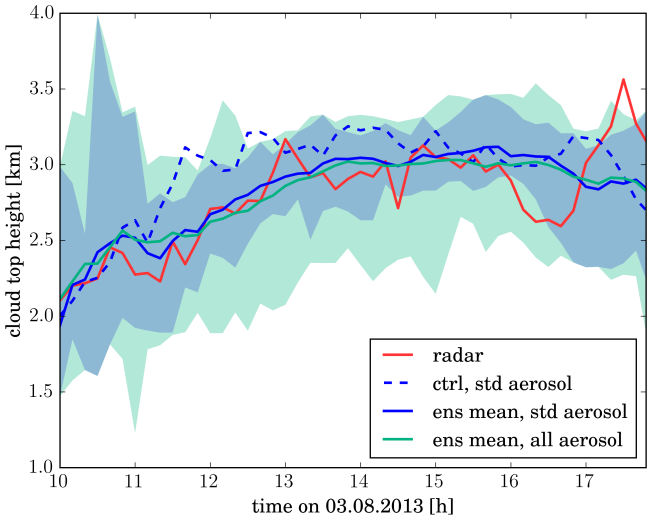


**Figure S3.** Comparison of cloud top height from the model simulation against radar data. Cloud top height is defined as the highest altitude at which the radar reflectivity reaches 18 dBZ. The red line represents the observational data, the dark blue dashed line the control run with the standard aerosol profile, the dark blue solid line the mean distribution from all ensemble members with the standard aerosol profile and the cyan line the mean distribution from all ensemble members with all aerosol profiles. The shaded regions display the spread between the ensemble members.

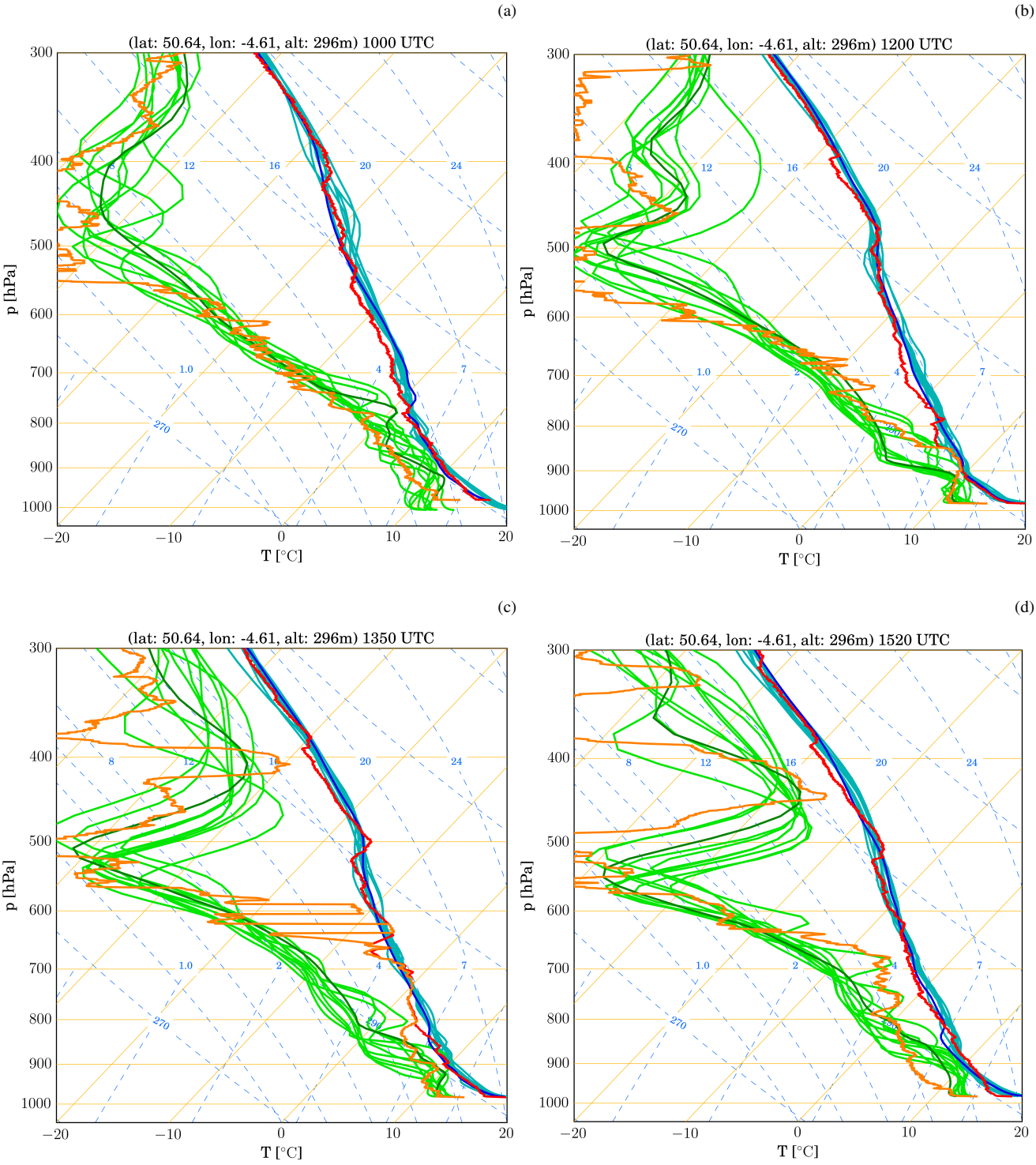


**Figure S4.** SkewT diagrams from radiosonde ascents at 1000 UTC (a), 1200 UTC (b), 1350 UTC (c) and 1520 UTC (d). The red (orange) curves show the observational data, while the different blue (green) curves show the temperature (dew-point temperature) profiles from the model grid column closest to the radiosonde release location for each ensemble member (standard aerosol profile).

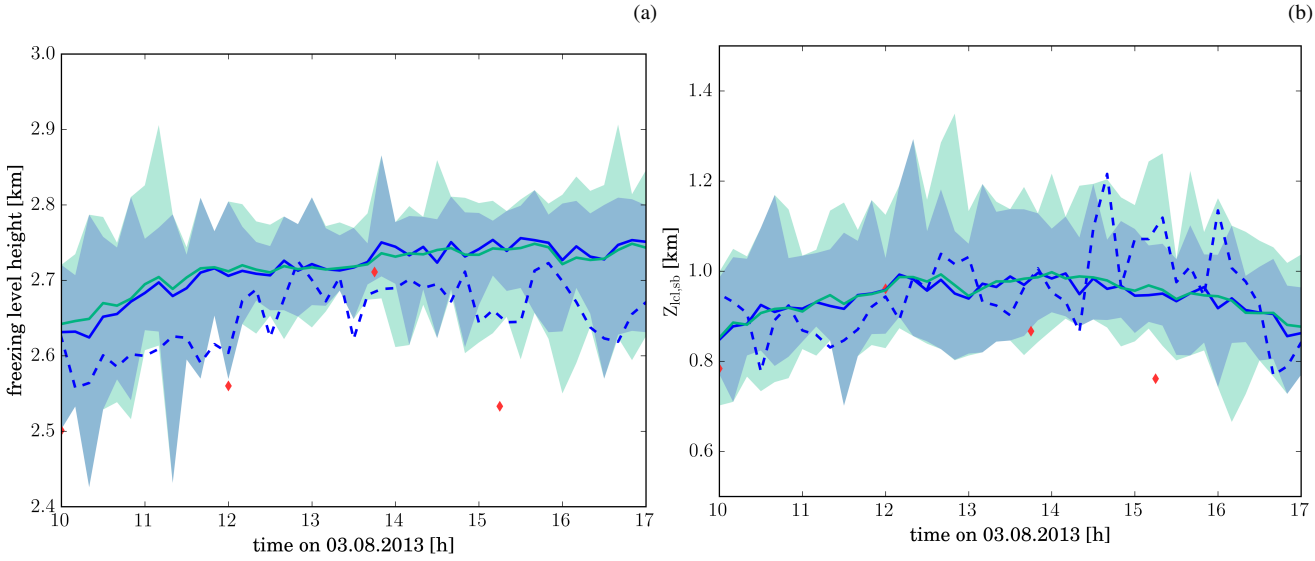


**Figure S5.** Time-series of freezing level height (a) and lifting condensation level (b) from the radiosondings at Davidstow and the closest model grid-column. The red diamonds represent the observational data, the dark blue dashed line the control run with the standard aerosol profile, the dark blue solid line the mean distribution from all ensemble members with the standard aerosol profile and the cyan line the mean distribution from all ensemble members with all aerosol profiles. The shaded regions display the spread between the ensemble members.

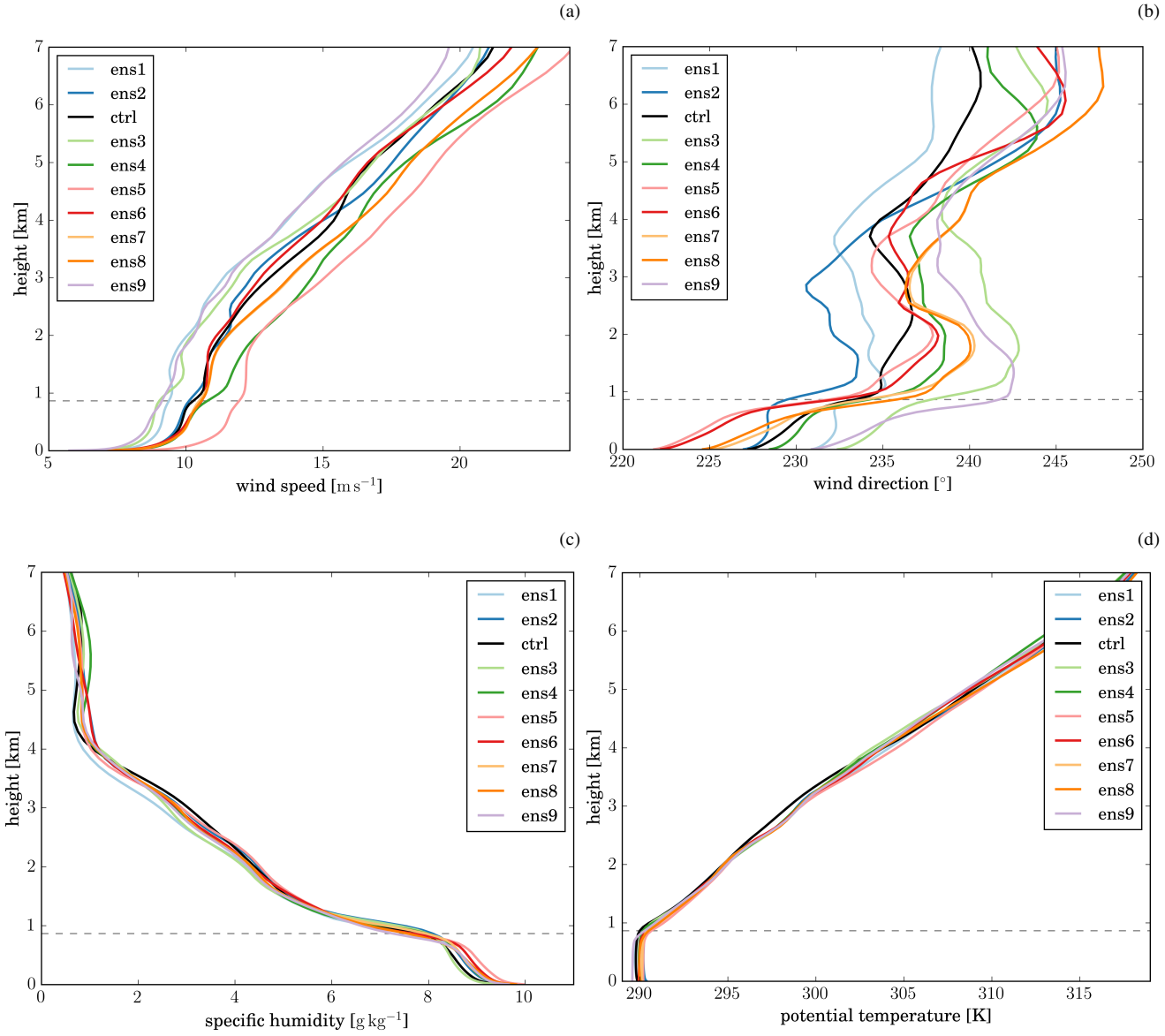


**Figure S6.** Comparison of upstream (western domain boundary) wind speed (a), wind direction (b), specific humidity (c), and potential temperature (d). The profiles are averaged over the time period between 10 UTC and 18 UTC. The different colours correspond to the individual ensemble members (including the control simulation).

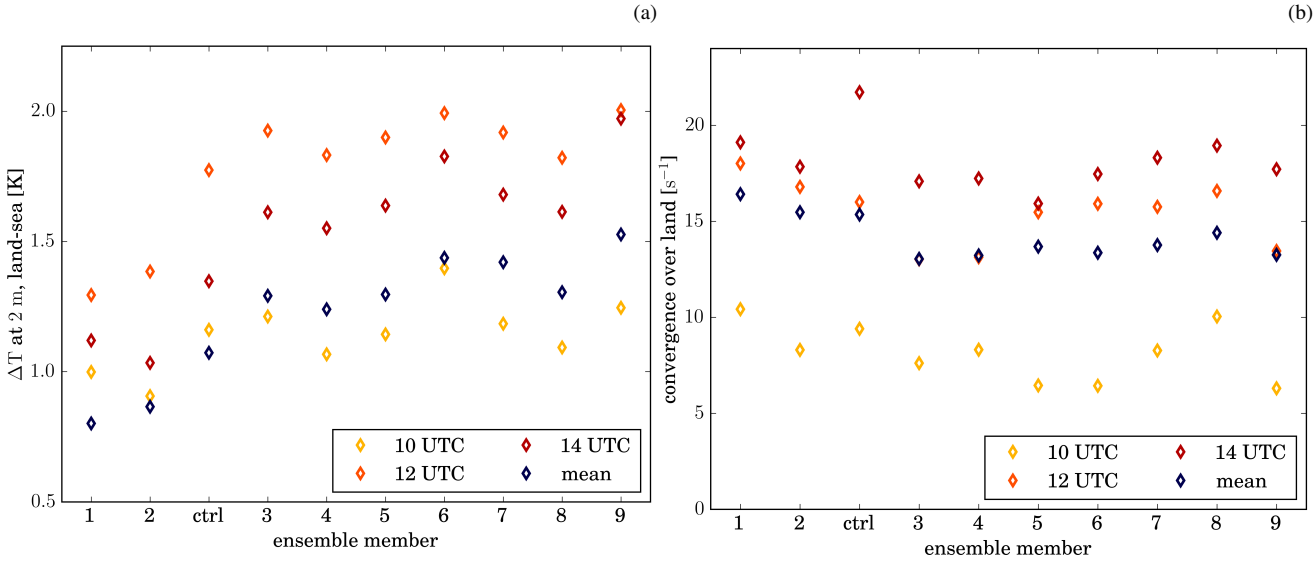


**Figure S7.** The temperature difference between land and sea is shown in panel (a) for different times (colours). The low-level convergence over the peninsula is displayed in panel (b). Only ensemble members using the standard aerosol profile are considered.

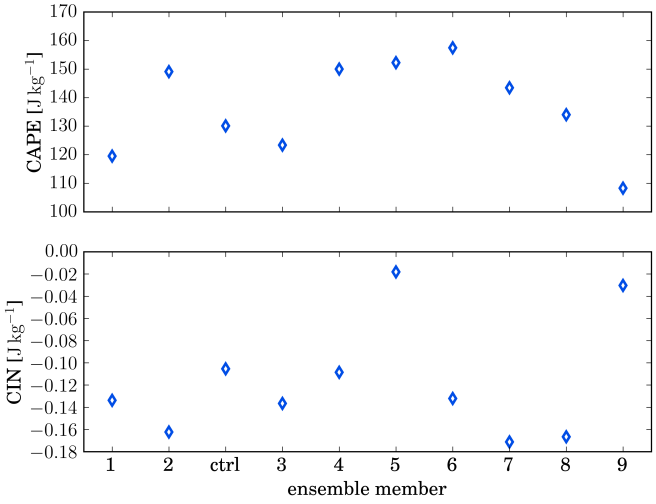


**Figure S8.** Average CAPE and CIN at upstream boundary for simulations with the standard aerosol profile.

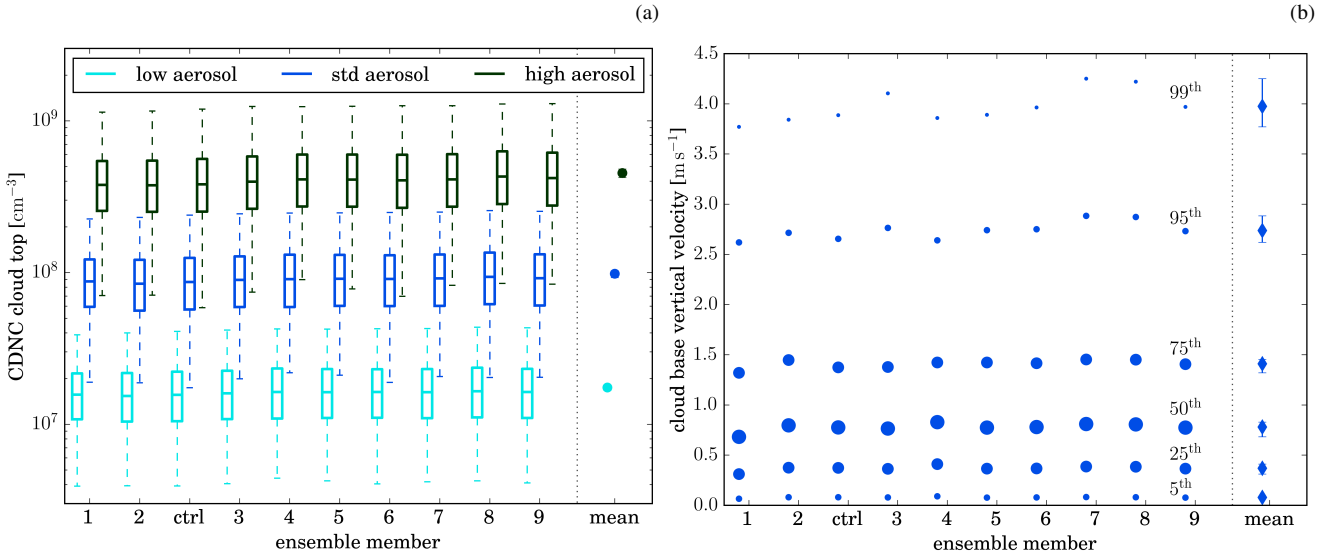


**Figure S9.** (a) Cloud droplet number concentration (CDNC) at cloud top for different ensemble members (abscissa) using different aerosol profiles (colours). CDNC at cloud top is computed as the average CDNC within 500 below the lowest highest) point in each grid column that has a cloud or ice mass mixing ratio larger than 1 $\mathrm{mg\,kg^{-1}}$. The horizontal line inside the boxes indicates the mean CDNC, the upper and lower edges the $25^{\text{th}}$ and $75^{\text{th}}$ percentile, respectively, and the whiskers the $1^{\text{st}}$ and $99^{\text{th}}$ percentile. The statistics are computed over all qualifying grid points in the domain between 0900 UTC and 1900 UTC and therefore reflect the spatial and temporal variability of CDNC. The last column provides the distribution of the ensemble means, with the dot representing the average of the ensemble means and the bars the spread of the ensemble means. (b) Percentiles of the cloud-base vertical velocity distribution for ensemble members with the standard aerosol scenario. The different percentiles are represented by differently sized circles.

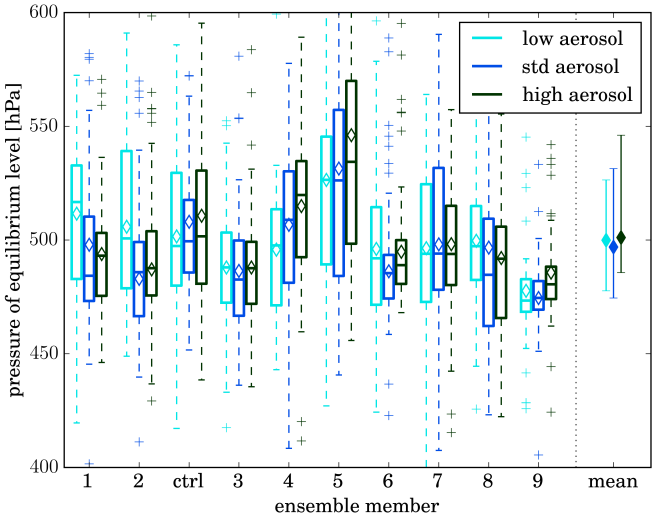


**Figure S10.** Pressure of equilibrium pressure level. The box plots represent the temporal variability of the variable.

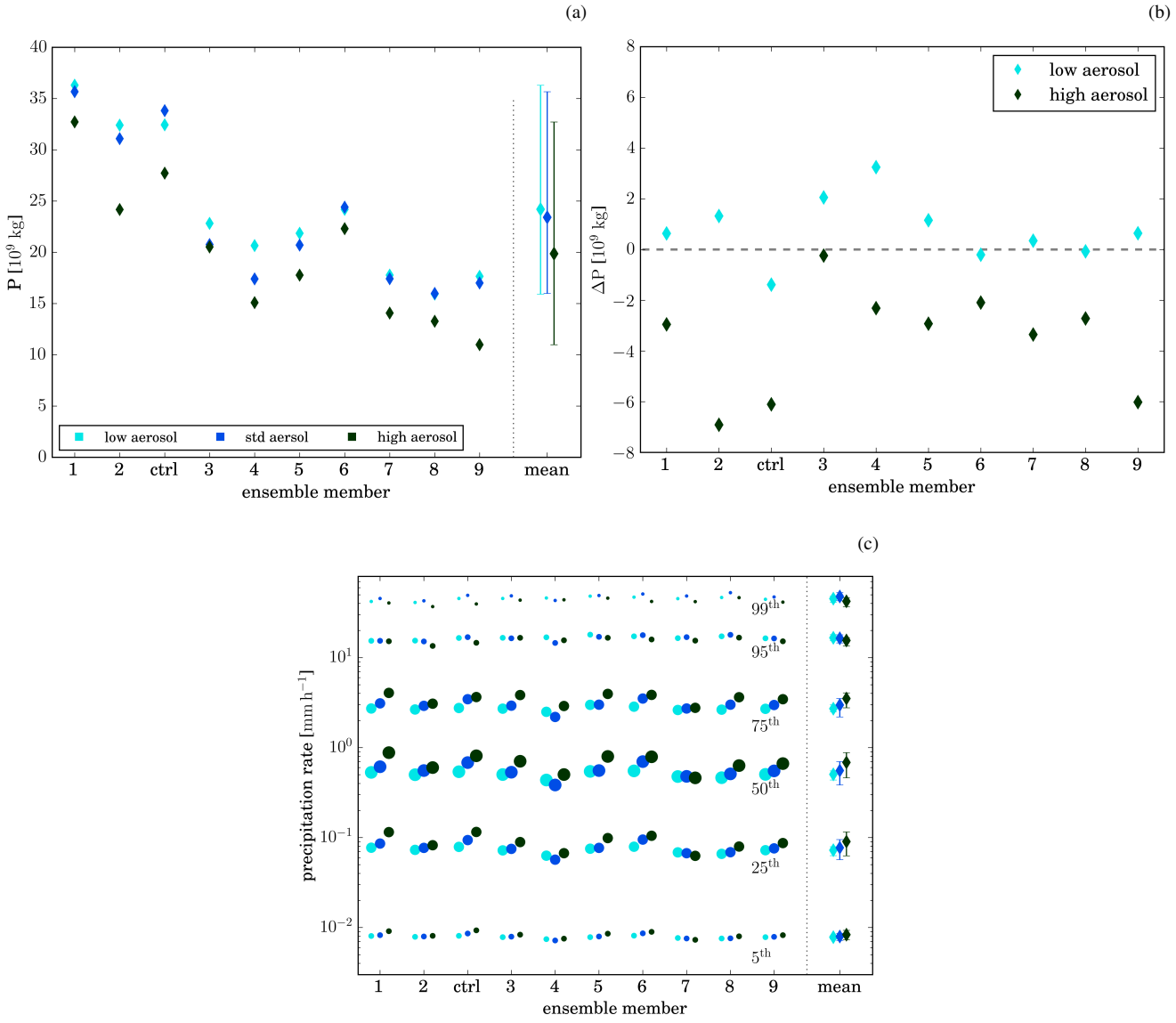


**Figure S11.** Accumulated surface precipitation over the time period $10 - 19$ UTC (a) and difference in accumulated surface precipitation relative to the ensemble member with the standard aerosol scenario (b). (c) Percentiles of the instantaneous rain rate. The $99^{\text{th}}$, $95^{\text{th}}$, $90^{\text{th}}$, $75^{\text{th}}$, $50^{\text{th}}$, $25^{\text{th}}$ and $5^{\text{th}}$ percentiles are shown from top to bottom. The different percentiles are represented by differently sized circles.

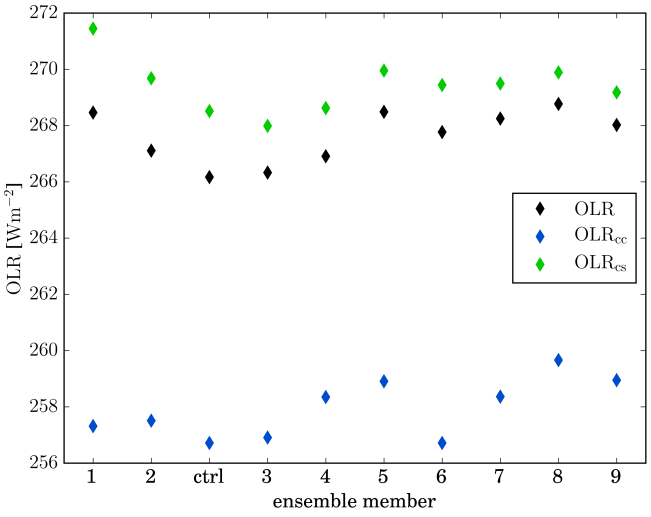


**Figure S12.** Mean outgoing longwave radiation from all grid points (top), from cloudy grid points only (middle) and from clear-sky grid points (bottom). Cloudy grid points have a total condensed water path larger than $1\,\mathrm{g\,m^{-2}}$.

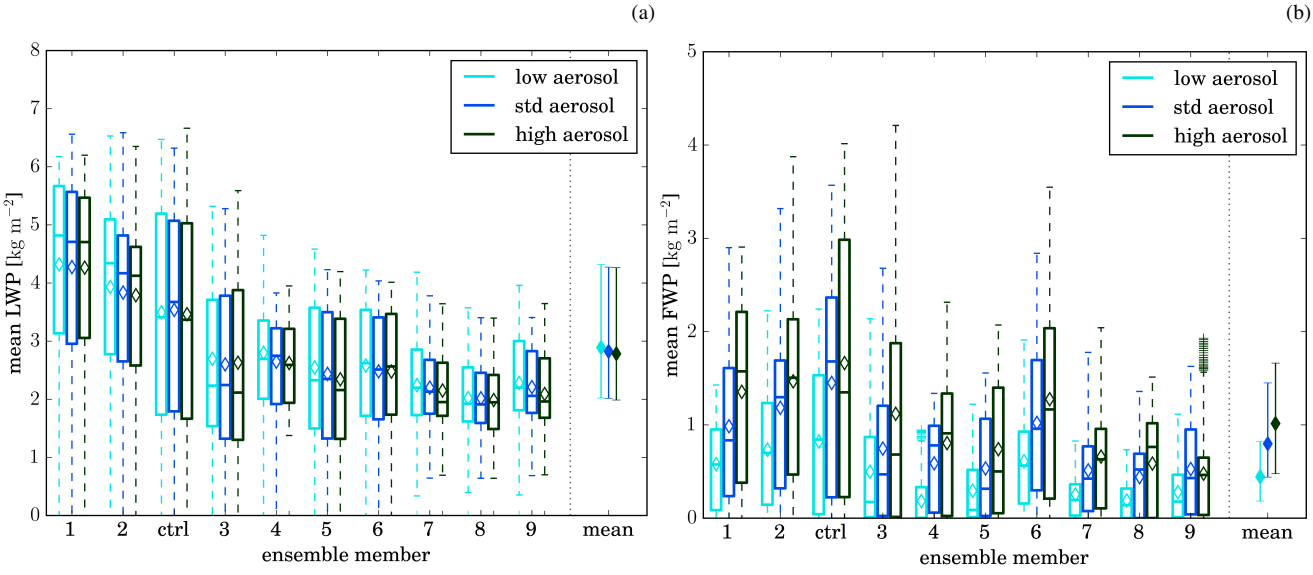


**Figure S13.** Mean liquid water path (cloud and rain) (b), and mean frozen water path (ice, snow and graupel) (c). The boxplots represent the temporal variability.

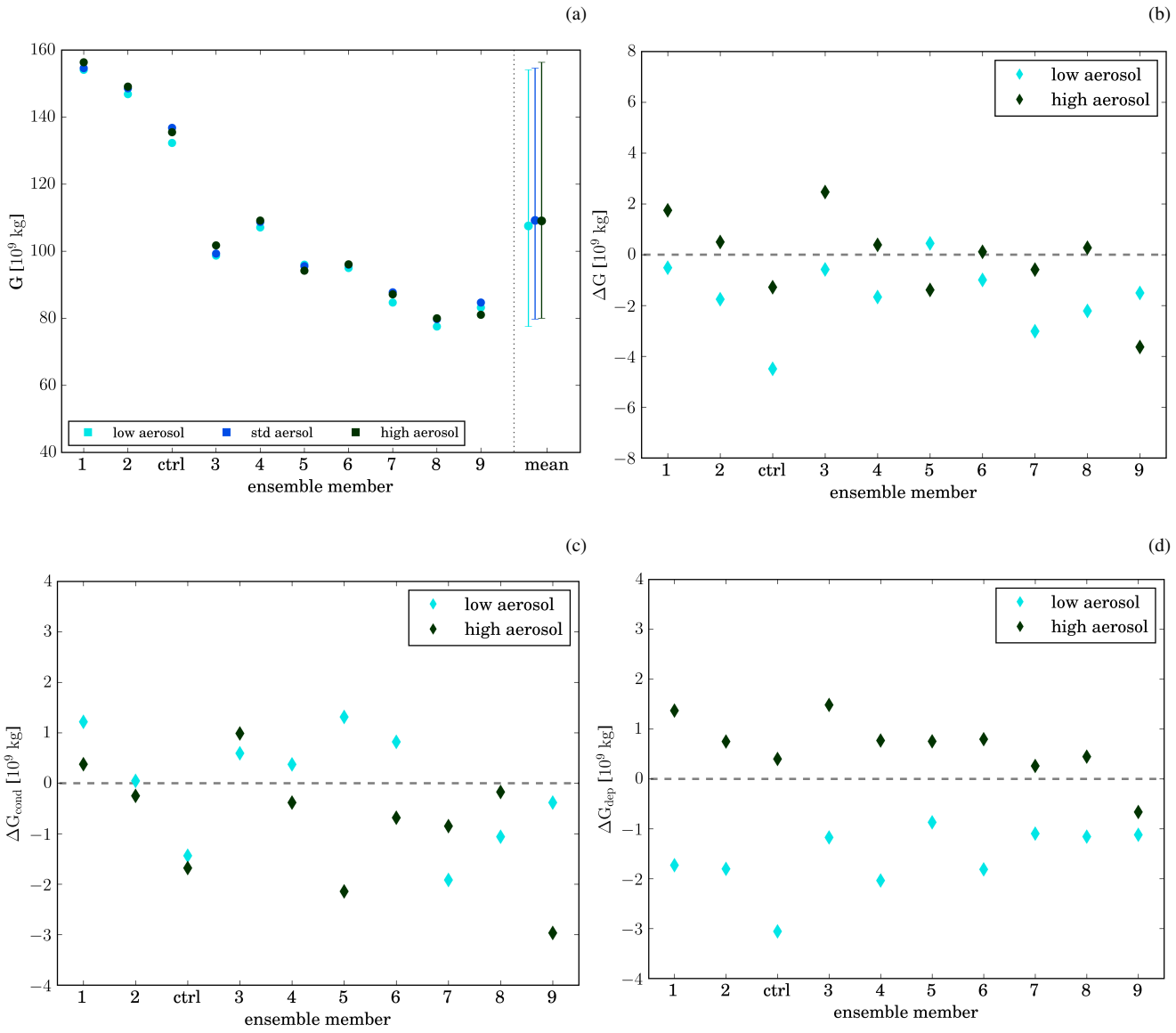


**Figure S14.** Accumulated condensate generation over the time period $10 - 19$ UTC (a), difference in condensate generation relative to the ensemble member with the standard aerosol scenario (b), and the difference in accumulated condensation rate (c) and accumulated deposition rate (d) relative to the standard aerosol run.

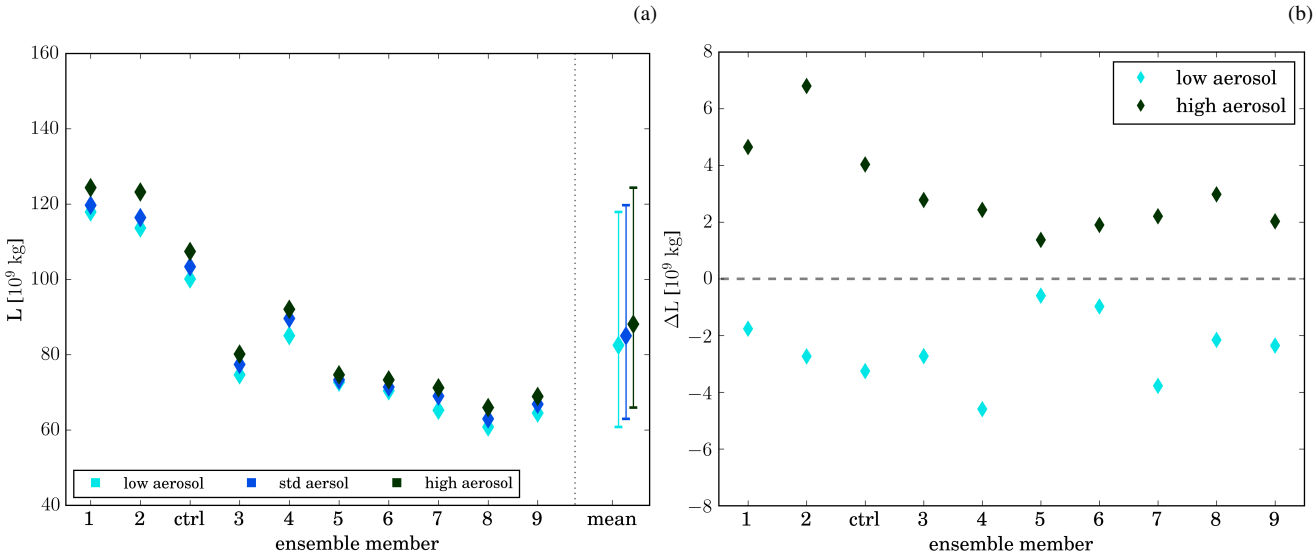


**Figure S15.** Accumulated condensate loss over the time period $10 - 19$ UTC (a) and difference in condensate loss relative to the ensemble member with the standard aerosol scenario (b).

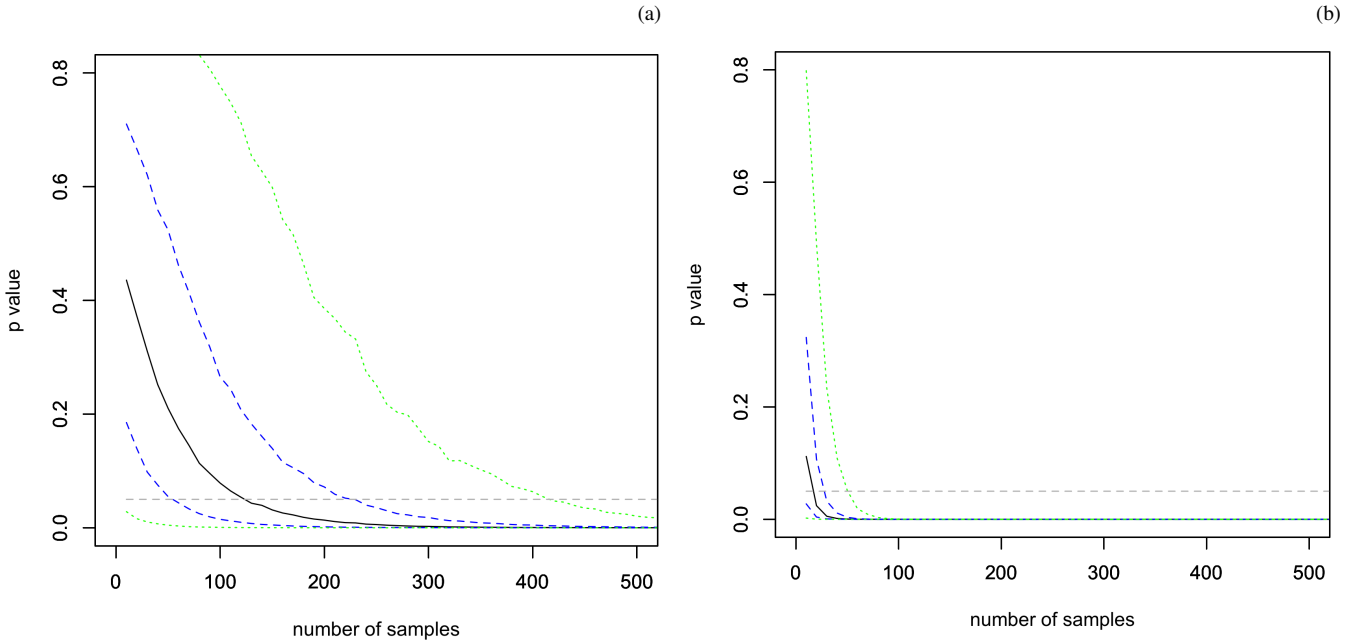


**Figure S16.** Statistical significance (p-value for two-sided t-test) of difference in accumulated surface precipitation between standard and low (a) and standard and high (b) aerosol scenario as a function of the number of observed days. The black solid line shows the median p-value from $10^4$ realisations, the dashed blue lines the $25^{\text{th}}$ and $75^{\text{th}}$ percentiles of the p-value, and the green dashed lines the $5^{\text{th}}$ and $95^{\text{th}}$.